

Quasiparticle interference on the surface of 3D topological insulator Bi_2Se_3 induced by cobalt adatom in the absence of ferromagnetic ordering

M. Ye,^{1,*} S. V. Eremeev,^{2,3} K. Kuroda,¹ E. E. Krasovskii,^{4,5,6} E. V. Chulkov,^{4,5} Y. Takeda,⁷ Y. Saitoh,⁷ K. Okamoto,¹ S. Y. Zhu,¹ K. Miyamoto,⁸ M. Arita,⁸ M. Nakatake,⁸ T. Okuda,⁸ Y. Ueda,⁹ K. Shimada,⁸ H. Namatame,⁸ M. Taniguchi,^{1,8} and A. Kimura^{1,†}

¹*Graduate School of Science, Hiroshima University,
1-3-1 Kagamiyama, Higashi-Hiroshima, 739-8526, Japan*

²*Institute of Strength Physics and Materials Science, 634021, Tomsk, Russia*

³*Tomsk State University, 634050, Tomsk, Russia*

⁴*Departamento de Física de Materiales UPV/EHU and Centro de
Física de Materiales CFM and Centro Mixto CSIC-UPV/EHU,
20080 San Sebastián/Donostia, Basque Country, Spain*

⁵*Donostia International Physics Center (DIPC),
20018 San Sebastián/Donostia, Basque Country, Spain*

⁶*IKERBASQUE, Basque Foundation for Science, 48011 Bilbao, Spain*

⁷*Condensed Matter Science Division, Japan Atomic Energy Agency, Sayo, Hyogo 679-5148, Japan*

⁸*Hiroshima Synchrotron Radiation Center, Hiroshima University,
2-313 Kagamiyama, Higashi-Hiroshima, 739-0046, Japan*

⁹*Kure National College of Technology, Agaminami 2-2-11, Kure 737-8506, Japan*

(Dated: August 24, 2018)

Quasiparticle interference induced by cobalt adatoms on the surface of the topological insulator Bi_2Se_3 is studied by scanning tunneling microscopy, angle-resolved photoemission spectroscopy and X-ray magnetic circular dichroism. It is found that Co atoms are selectively adsorbed on top of Se sites and act as strong scatterers at the surface, generating anisotropic standing waves. A long-range magnetic order is found to be absent, and the surface state Dirac cone remains gapless. The anisotropy of the standing wave is ascribed to the heavily warped iso-energy contour of unoccupied states, where the scattering is allowed due to a non-zero out-of-plane spin.

PACS numbers:

A novel class of materials, called topological insulators (TI) [1–3] with a nontrivial metallic surface state in the bulk energy gap induced by spin-orbit coupling have invoked both theoretical and experimental interest.. An odd number of surface states with a spin helical texture established for $\text{Bi}_{1-x}\text{Sb}_x$ [4, 5], Bi_2Te_3 [6], Bi_2Se_3 [7, 8], and TI-based ternary compounds [9–14] promises a robust protection of spin polarized surface states from backscattering in the presence of non-magnetic impurities due to time-reversal (TR) symmetry, which is a key requirement to revolutionize modern electronic devices. Among discovered TI materials, Bi_2Se_3 is one of the most promising candidates owing to the large bulk energy gap with a single Dirac cone surface state.

In fact, a spin-selective scattering has been directly imaged by scanning tunneling microscopy (STM) even without the breaking of TR symmetry [5, 15, 16]. Especially for Bi_2Te_3 , a suppressed backscattering of topological surface electrons by nonmagnetic impurities has been reported [15]. It should be noted that owing to the relatively small size of bulk energy gap and a strong

anisotropy of the bulk band structure, the topological surface state of Bi_2Te_3 is strongly hexagonally warped [16, 17], which leads to the quasiparticle interference (QPI) with scattering vector along the $\bar{\Gamma}$ - \bar{M} direction between states with out-of-plane spin components [15], even though the backscattering is strictly forbidden due to the TR symmetry. In other words, more favorable protection would be realized in TI materials with larger bulk energy gap, such as Bi_2Se_3 .

Most interesting properties appear when the surfaces of 3D TIs are interfaced with ferromagnetic layers [18–22]. Due to a broken TR symmetry, an energy gap opens at the Dirac point, leading to massive Dirac fermions. In such a system novel physical phenomena are expected to emerge, in particular the half quantum Hall effect on the surface with a Hall conductance of $e^2/2h$ [23], as well as the Kondo effect mediated by the Dirac fermions [24].

Experimentally, great efforts have been made on the magnetic doping in the bulk of TI materials. An opening of the energy gap at Dirac point and the consequent QPI on the topological surface due to the broken TR symmetry have been directly observed [25, 26]. On the other hand, the magnetic doping at the surface, which can be realized by the deposition of magnetic atoms, is still poorly explored although it is expected to stronger influence the surface Dirac fermions than

*Present address: Hiroshima Synchrotron Radiation Center, Hiroshima University, Japan.

†Electronic address: akiok@hiroshima-u.ac.jp

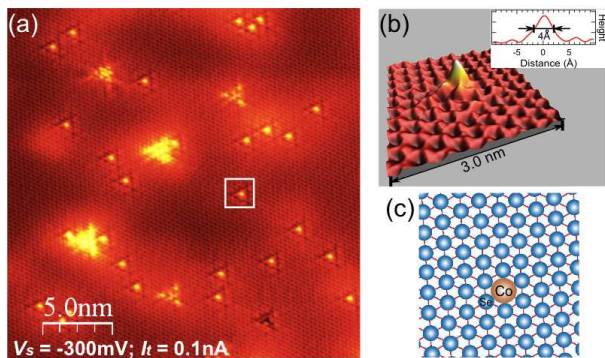


FIG. 1: (Color online) (a) STM image of Co deposited Bi_2Se_3 surface ($25\text{nm} \times 25\text{nm}$). (b) 3D illustration of a Co adatom (a), inset, cross-sectional profile of the Co adatom on Bi_2Se_3 . (c) Schematics of atomic structure in (b).

the bulk doping [27, 28]. Here we show for the first time that Co atoms on the surface of Bi_2Se_3 generate a distinct QPI of the surface Dirac fermions without opening of an energy gap at the Dirac point. The absence of a long-range ferromagnetic order is revealed by combined STM, angle-resolved photoemission spectroscopy (ARPES), and x-ray magnetic circular dichroism (XMCD) experiments.

Our measurements were performed on the pristine Bi_2Se_3 single crystal, which is naturally n-type. Clean surfaces were obtained by *in-situ* cleavage in ultra-high vacuum at room temperature. Cobalt deposition was made at room temperature after the confirmation of the clean surface by STM. The present STM results were obtained at 4.7 K in the constant current mode, and the differential conductance (dI/dV) map was acquired by a standard lock-in technique. ARPES experiments were performed at BL-7 of Hiroshima Synchrotron Radiation Center equipped with a hemispherical photoelectron analyzer (VG-SCIENITA SES2002). XMCD experiment on Co deposited Bi_2Se_3 surface was conducted at the twin helical undulator beam line BL23SU of SPring-8 in a total-electron yield mode, employing a superconducting magnet and a helium cryostat.

Figure 1(a) shows a typical STM image acquired at a sample bias voltage of $V_s = -300\text{ mV}$ of the Co-deposited Bi_2Se_3 surface. Two kinds of bright features can be identified in the image, namely the large triangular-shaped patterns and the tiny bright spots. The large features are typically found in both Bi_2Se_3 and Bi_2Te_3 surfaces and are assigned as the substitutional or antisite defect [29–31]. The tiny bright spots appear after the Co deposition and are assigned as Co adatoms. A close-up STM image of the Co adatom [marked with white frame in Fig. 1(a)] is shown in Fig. 1(b). The 3D illustration of the Co adatom in Fig. 1(b) clearly shows the sharp protrusion on the surface with a spatial full

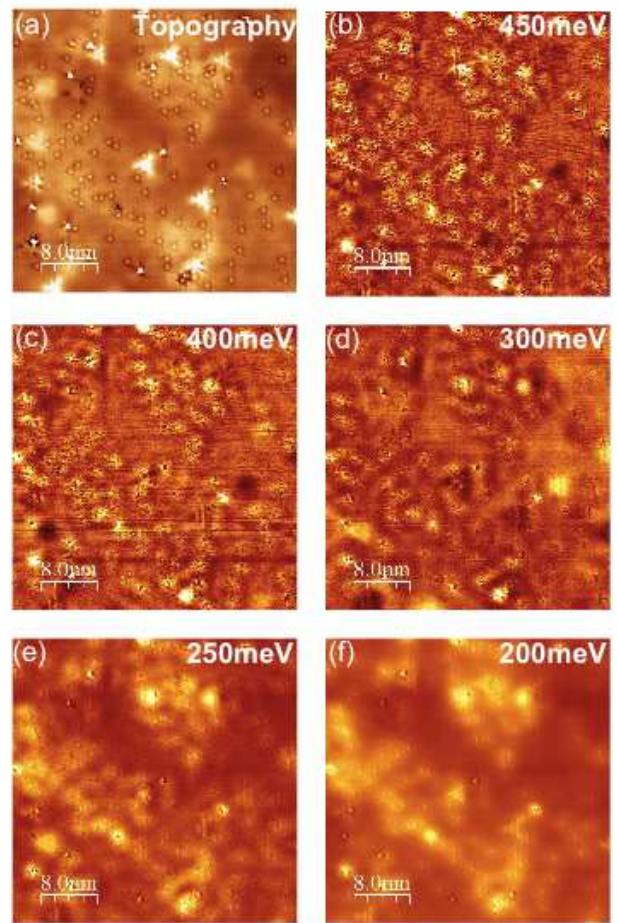


FIG. 2: (Color online) (a) $40\text{nm} \times 40\text{nm}$ area STM image of Co evaporated Bi_2Se_3 surface (sample bias 300mV , set point 0.10nA); (b)-(f) dI/dV images taken at the same area as (a) with different sample bias voltages (set pint 0.10nA)

width at half maximum of 4 \AA [inset of Fig. 1(b)]. By carefully examining the atomic position in this area we identify the Co adatom as located on the top of the Se atom, as schematically shown in Fig. 1(c).

Figure 2(a) shows a topographic STM image in a $40\text{ nm} \times 40\text{ nm}$ area. In the measured set of dI/dV images with different sample bias voltages clear QPI features around the Co adatoms are observed. The QPI standing wave gradually changes its wave length depending on V_s , see Figs. 2(b)-2(f). As V_s decreases, the wavelength in the real space (r -space) increases. For $V_s < 200\text{ mV}$, the interference patterns become rather diffuse. Moreover, the standing waves observed around the Co adatoms exhibit strong anisotropic shape, in contrast to what is commonly observed at high-index surfaces of pure metals [32, 33].

To gain a deeper insight into the relationship between the interference pattern and V_s , the real space dI/dV

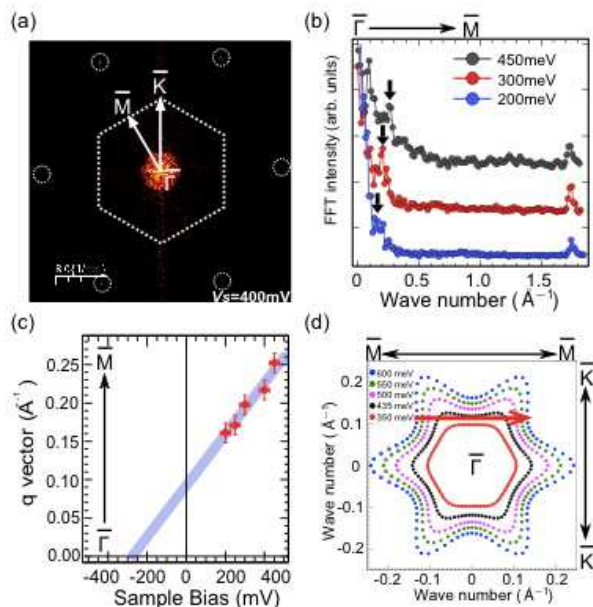


FIG. 3: (Color online) (a) Fourier transformed dI/dV images acquired at $V_S = 400$ mV, surface Brillouin zone is indicated by the white dashed hexagon. (b) Profile curves of Fourier transformed image along $\bar{\Gamma}$ - \bar{M} at different sample bias voltages. (c) Plot of the interference peak along $\bar{\Gamma}$ - \bar{M} direction (indicated by an arrow in (c)) as a function of sample bias voltages. (d) Calculated constant energy contour of Bi_2Se_3 , the red arrow indicates the scattering channel along $\bar{\Gamma} - \bar{K}$ due to the perpendicular spin component.

maps are Fourier transformed, as depicted in Fig. 3(a) for the sample bias voltage of 400 mV. The six spots marked with white dashed circles are (1×1) spots in the reciprocal space, and the $(0, 0)$ spot is located in the center of the image. The surface Brillouin zone is shown in Fig. 3(a) as a hexagon with the $\bar{\Gamma}$ point located in the center. The reciprocal space image in Fig. 3(a) reveals the anisotropic interference patterns with six-fold symmetry. The intensity maximum is in the $\bar{\Gamma}$ - \bar{M} direction as shown by the cross-sectional profiles at different sample bias voltages in Fig. 3(b). The six-fold pattern gradually shrinks with decreasing V_s and eventually vanishes below 200 mV, as indicated by arrows in Fig. 3(b). Further quantitative analysis reveals that wave number of the peak in the cross-sectional profiles along $\bar{\Gamma}$ - \bar{M} almost linearly shifts with V_s [Fig. 3(c)].

In case that the TR symmetry is broken, the appearance of the energy gap at the Dirac point would simultaneously result in the opening of the scattering channels at all energies. Thus, the vanishing of the standing waves below 200 mV in the dI/dV map, where the warping effect of Dirac cone becomes neglectable, suggests that the TR protection of the topological surface state persists without a gap opening at the Dirac point even in the presence of Co impurities. The

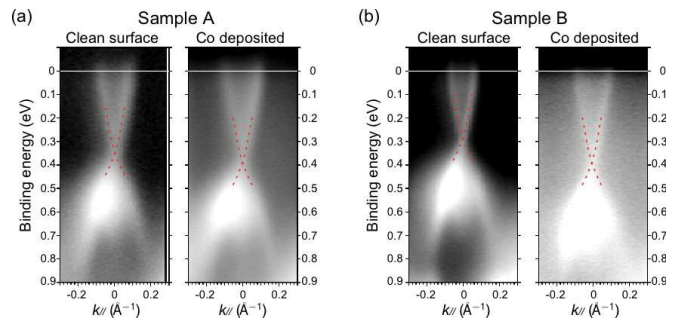


FIG. 4: (Color online) ARPES measurement on two samples before and after (a) 0.2 ML and (b) 0.9 ML of Co deposited acquired by photon energy of 50 eV.

scattering observed with large sample bias voltages in the unoccupied states can be ascribed to a heavily deformed iso-energy contour in the high energy range (the unoccupied states) as indicated by the scattering vector superimposed on the calculated constant energy contours in Fig. 3(d). The scattering channel is allowed because of the finite surface perpendicular spin component [8, 34].

To see how the surface states dispersion is modified upon Co deposition, we have employed ARPES with synchrotron radiation. Two sets of measurements were performed with different Co deposition durations on two samples labeled A and B. Here, we use the photon energy of 50 eV, at which the spectral weight of the bulk conduction band is largely suppressed and the surface Dirac cone is highlighted.

For both samples, the linear surface state dispersion is clearly observed before as well as after the Co deposition, but the background is stronger with larger Co coverage. For the sample A [Fig. 4(a)], the Dirac point prior to the Co deposition is located at 340 meV below the Fermi level. After 0.2 ML Co deposition, the Dirac point shifts to 390 meV, and no other significant changes of the Dirac cone is observed. When the amount of Co increases to 0.9 ML (sample B, Fig. 4(b)), a larger energy shift of ~ 100 meV is observed with stronger background intensity. Again, neither the change of spectral feature nor the energy gap opening is observed. These results imply either the absence of the ferromagnetic order or the vanishing of the magnetic moment of Co atoms deposited on the surface of Bi_2Se_3 , which may be ascribed to the chemical bonding with Se atoms on the topmost layer. Thus, the QPI observed in the present STM results should be originated from the deformation of the Fermi surface [8, 34] rather than from a broken TR symmetry.

Finally, to understand the magnetic properties of Co on the surface of Bi_2Se_3 , we have performed X-ray magnetic circular dichroism measurement, which is able to resolve element-specific magnetic properties. Figure 5(a) shows the Co L_{23} X-ray absorption spectra (XAS) for three different coverages. Also the absorption

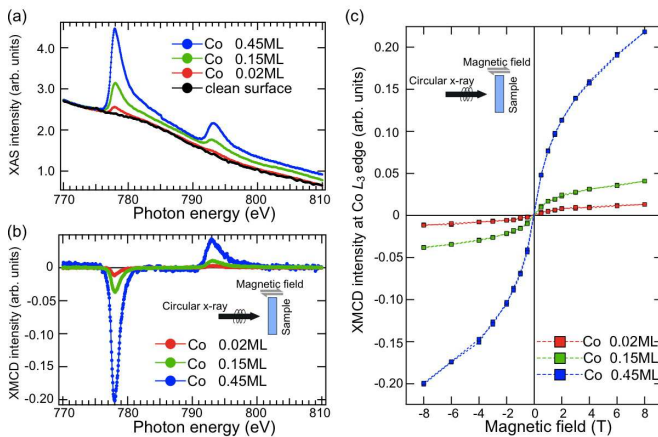


FIG. 5: (Color online) (a) XAS, (b) XMCD spectra at Co L_{23} edges, and (c) site-specific magnetization measurement of Co L_3 edge with different coverage of Co on Bi_2Se_3 surface (temperature, 5 K).

spectrum of the clean sample is measured to estimate the background contribution. As can be seen in Fig. 5(a), when the coverage of Co increases from 0.02 to 0.45 ML, the total absorption intensities at 778 and 793 eV gradually increase. The XMCD spectrum is obtained by measuring the difference of the absorption intensities with the circular polarization vector of the incident light parallel and anti-parallel to the magnetic field. Figure 5(b) shows the XMCD spectra acquired under 8 Tesla magnetic field applied perpendicular to the sample surface at 5 K. The intensity of XMCD signal of both L_3 and L_2 edges increases with increasing Co coverage. Note that the ratio between the orbital and spin magnetic moment deduced from the XMCD spectra of the Co layer deposited on Bi_2Se_3 ($m_{\text{orb}}/m_{\text{spin}} \sim 0.3\text{--}0.5$) is for the three measured Co coverages considerably larger than for the bulk Co crystal ($m_{\text{orb}}/m_{\text{spin}} \sim 0.1$) [35].

Whether the Co deposited Bi_2Se_3 surfaces are ferromagnetic or not can be inferred by investigating site-specific magnetization as a function of magnetic field. Figure 5(c) shows the intensity of XMCD signal at Co L_3 edges as a function of the magnetic field (M-H curve), which is swept from -8 to 8 T and then back to -8 T to form a loop. As is seen from Fig. 5(c), the M-H curves for all the three coverages of Co increase in the same direction with increasing the magnetic field strength. However, the intensity of the M-H curves are not saturated even at 8 T and no magnetic hysteresis is observed for any of the three Co coverages. These results clearly show that the Co layer on the Bi_2Se_3 surface has no long-range ferromagnetic order. This is consistent with our ARPES results, which show no gap-opening at the Dirac point upon Co deposition, and, thereby, confirm that the QPI patterns observed in the STM experiment originate from the strongly warped Dirac

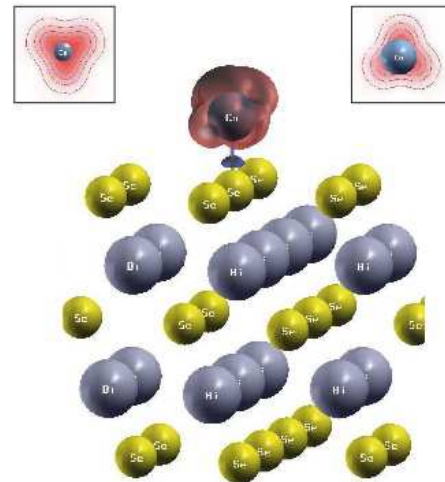


FIG. 6: (Color online) Constant-density surface for perpendicular (z) magnetization density (red and blue colors correspond to positive and negative values, respectively). Insets show cross-sections of this surface in xy plane just above (left) and below (right) the Co atom center.

cone in the unoccupied states of Bi_2Se_3 .

In order to further investigate the magnetic state of cobalt on the surface, we have performed *ab initio* DFT calculations using the VASP code [36–38]. We considered a single Co adatom within a slab model of a 3×3 surface super-cell of Bi_2Se_3 . The lateral position of the atom was fixed to be above the Se atom in accordance with our STM data, and the height of the Co atom above the top Se atom was optimized to be 2.27 Å (within a collinear scalar-relativistic approximation). The magnetic properties of the Co adatom in this position were calculated with the inclusion of the spin-orbit coupling. The magnetic moment of the Co adatom is found to be $2.06 \mu_B$ along the z axis. At the same time, the magnetic adatom does not induce a noticeable spin polarization of the substrate. The calculated z -magnetization density is shown in Fig. 6. The obtained negligible polarization of the substrate explains why the magnetic interaction between the adsorbed Co atoms is extremely weak, and why no ferromagnetic ordering at a low Co coverage is observed in the experiment.

In summary, by measuring the bias-dependent differential conductance mapping we have observed the QPI of Dirac electrons induced by Co impurities in the unoccupied states of Bi_2Se_3 . The magnetic properties of Co deposited Bi_2Se_3 surfaces investigated by XMCD reveal an absence of ferromagnetism, in agreement with our ARPES results that the Dirac point of the topological surface state is not destroyed by the Co impurities. We conclude that the QPI near Co impurities originates from the strongly deformed isoenergy contours of the

unoccupied states of Bi_2Se_3 . The present results may also provide a pathway to future studies of Kondo physics in the presence of the topological surface electrons.

STM and ARPES measurements were performed with the approval of the Proposal Assessing Committee of HSRC (Proposal No.11-B-40, No.10-A-32). The XMCD experiment was performed at SPring-8 with the approval of Japan Atomic Energy Agency (JAEA) as Nanotechnology Network Project of the Ministry of Education, Culture, Sports, Science and Technology. (Proposal No. 2011A3873/BL23SU). This work was partly supported by KAKENHI (No. 20340092, 23340105), Grant-in-Aid for Scientific Research (B) of Japan Society for the Promotion of Science. Author MY thanks financial support from JSPS Research Fellowship.

-
- [1] M. Z. Hasan and C. L. Kane, *Rev. Mod. Phys.* **82**, 3045-3067 (2010).
- [2] D. Hsieh, *et al.*, *Nature* **452**, 970 (2008).
- [3] Haijun Zhang, *et al.*, *Nature Phys.* **5**, 438 (2009).
- [4] D. Hsieh, *et al.*, *Science* **323**, 919 (2009).
- [5] Pedram Roushan, *et al.*, *Nature* **460**, 1106 (2009).
- [6] Y. L. Chen, *et al.*, *Science* **325**, 178 (2009).
- [7] Y. Xia, *et al.*, *Nature Phys* **5**, 398 (2009).
- [8] K. Kuroda, *et al.*, *Phys. Rev. Lett.* **105**, 076802(2010).
- [9] S. V. Eremeev, Yu. M. Koroteev, and E.V.Chulkov, *JETP. Lett.* **91**, 594 (2010).
- [10] K. Kuroda, *et al.* *Phys. Rev. Lett.* **105**, 146801 (2010).
- [11] S. V. Eremeev, G. Bihlmayer, M. Vergniory, Yu. M. Koroteev, T. V. Menshchikova, J. Henk, A. Ernst, and E. V. Chulkov, *Phys. Rev. B* **83**, 205129 (2011).
- [12] B. Yan, *et al.* *Europhys. Lett.* **90**, 37002 (2010).
- [13] H. Lin, *et al.* *Phys. Rev. Lett.* **105**, 036404 (2010).
- [14] T. Sato, *et al.* *Phys. Rev. Lett.* **105**, 136802 (2010).
- [15] Tong Zhang, *et al.*, *Phys. Rev. Lett.* **103**, 266803 (2009).
- [16] Zhanybek Alpichshev, *et al.*, *Phys. Rev. Lett.* **104**, 016401 (2010).
- [17] Wei-Cheng Lee, Congjun Wu, Daniel P. Arovas, and Shou-Cheng Zhang, *Phys. Rev. B* **80**, 245439 (2009).
- [18] Xiao-Liang Qi, Rundong Li, Jiadong Zang, and Shou-Cheng Zhang, *Science* **323**, 1184 (2009).
- [19] Rui Yu, *et al.*, *Science* **329**, 61 (2010).
- [20] R.R. Biswas, and A.V. Balatsky, *Phys. Rev. B* **81**, 233405 (2010).
- [21] I. Garate, and M. Franz, *Phys. Rev. Lett.* **104**, 146802 (2010).
- [22] V.N. Men'shov, V.V. Tugushev, and E.V. Chulkov, *Pis'ma v ZhETF.* **94**, 672 (2011).
- [23] Xiao-Liang Qi, Taylor L. Hughes, and Shou-Cheng Zhang *Phys. Rev. B* **78**, 195424 (2008).
- [24] T. O. Wehling, *et al.*, *Phys. Rev. B* **81**, 115427 (2010).
- [25] Y. L. Chen, *et al.*, *Science* **329** 659 (2010).
- [26] Y. Okada, *et al.*, *Phys. Rev. Lett.* **106** 206805 (2011).
- [27] Qin Liu, *et al.*, *Phys. Rev. Lett.* **102**, 156603 (2009).
- [28] L.A. Wray, *et al.*, *Nature Phys.* **7**, 32 (2010).
- [29] S. Urazhdin, *et al.*, *Phys. Rev. B* **66**, 161306 (2002).
- [30] Guang Wang, *et al.*, *Adv. Mater.* **23**, 1162 (2011).
- [31] S. Kim, *et al.*, *Phys. Rev. Lett.* **107**, 056803 (2011)
- [32] M. F. Crommie, C. P. Lutz, and D. M. Eigler, *Nature (London)* **363**, 524 (1993).
- [33] Y. Nishimura, *et al.*, *Phys. Rev. B* **79**, 245402 (2009).
- [34] Liang Fu, *Phys. Rev. Lett.* **103**, 266801 (2009).
- [35] C. T. Chen, *et al.*, *Phys. Rev. Lett.* **75**, 152 (1995).
- [36] G. Kresse, J. Hafner, *Phys. Rev. B* **48**, 13115 (1993).
- [37] G. Kresse, J. Furthmüller, *Comput. Mater. Sci.* **6**, 15 (1996).
- [38] G. Kresse, D. Joubert, *Phys. Rev. B* **59**, 1758 (1998).